THE JOURNAL OF BIOLOGICAL CHEMISTRY VOL. 282, NO. 43, pp. 31580–31591, October 26, 2007
© 2007 by The American Society for Biochemistry and Molecular Biology, Inc. Printed in the U.S.A.

Kinetic Resolution of a Tryptophan-radical Intermediate in the Reaction Cycle of *Paracoccus denitrificans* Cytochrome *c* Oxidase*[S]

Received for publication, July 5, 2007, and in revised form, August 17, 2007 Published, JBC Papers in Press, August 30, 2007, DOI 10.1074/jbc.M705520200

Frank G. M. Wiertz[‡], Oliver-Matthias H. Richter[§], Bernd Ludwig[§], and Simon de Vries[‡1]

From the [‡]Department of Biotechnology, Delft University of Technology, Julianalaan 67, Delft 2628 BC, The Netherlands and the [§]Molecular Genetics Group, Institute of Biochemistry, and Cluster of Excellence Macromolecular Complexes, J. W. Goethe Universität, Max-von Laue-Strasse 9, Frankfurt am Main D-60438, Germany

The catalytic mechanism, electron transfer coupled to proton pumping, of heme-copper oxidases is not yet fully understood. Microsecond freeze-hyperquenching single turnover experiments were carried out with fully reduced cytochrome aa_3 reacting with O_2 between 83 μs and 6 ms. Trapped intermediates were analyzed by low temperature UV-visible, X-band, and Q-band EPR spectroscopy, enabling determination of the oxidation-reduction kinetics of Cu_A, heme *a*, heme a_3, and of a recently detected tryptophan radical (Wiertz, F. G. M., Richter, O. M. H., Cherepanov, A. V., MacMillan, F., Ludwig, B., and de Vries, S. (2004) *FEBS Lett.* 575, 127–130). Cu_B and heme a_3 were EPR silent during all stages of the reaction. Cu_A and heme *a* are in electronic equilibrium acting as a redox pair. The reduction potential of Cu_A is 4.5 mV lower than that of heme *a*. Both redox groups are oxidized in two phases with apparent half-lives of 57 μs and 1.2 ms together donating a *single* electron to the binuclear center in each phase. The formation of the heme a_3 oxoferryl species P_R (maxima at 430 nm and 606 nm) was completed in ~130 μs, similar to the first oxidation phase of Cu_A and heme *a*. The intermediate *F* (absorbance maximum at 571 nm) is formed from P_R and decays to a hitherto undetected intermediate named F_W*. F_W* harbors a tryptophan radical, identified by Q-band EPR spectroscopy as the tryptophan neutral radical of the strictly conserved Trp-272 (Trp-272*). The Trp-272* populates to 4–5% due to its relatively low rate of formation ($t_{½}$ = 1.2 ms) and rapid rate of breakdown ($t_{½}$ = 60 μs), which represents electron transfer from Cu_A/heme *a* to Trp-272*. The formation of the Trp-272* constitutes the major rate-determining step of the catalytic cycle. Our findings show that Trp-272 is a redox-active residue and is in this respect on an equal par to the metallocenters of the cytochrome *c* oxidase. Trp-272 is the direct reductant either to the heme a_3 oxoferryl species or to Cu_B^{2+}. The potential role of Trp-272 in proton pumping is discussed.

The superfamily of heme-copper oxidases comprises the cytochrome oxidases, which catalyze the reduction of molecular oxygen to water and the NO reductases that catalyze the reduction of NO to N_2O (1–6). Cytochrome oxidases (CcOs)[2] are the final electron acceptors in the respiratory chains of bacteria, archaea, and mitochondria. Cytochrome aa_3 from *Paracoccus denitrificans*, is a Type A oxidase based on the structure of its D- and K-proton pathways (7, 8). The reduction of oxygen (Reaction 1) generates a proton electrochemical gradient across the cytoplasmic membrane. Four protons are used for the formation of water, and four are pumped across the membrane according to,

$$4\text{cyt } c^{2+} + O_2 + 8H_C^+ \rightarrow 4\text{cyt } c^{3+} + 2H_2O + 4H_P^+$$

REACTION 1

where H_C^+ are protons taken up from the cytoplasm and H_P^+ protons are those ejected to the periplasm (9–13).

The crystal structures of cytochrome aa_3 from bovine heart mitochondria, *P. denitrificans*, and *Rhodobacter sphaeroides* have been solved previously (8, 14–18). *P. denitrificans* cytochrome aa_3 is a four-subunit membrane complex. Subunit one harbors heme *a* and the heme a_3-Cu_B binuclear reaction center where reduction of oxygen takes place. Subunit two contains the docking site for cytochrome *c* (19, 20) and the Cu_A mixed-valence binuclear center with two copper atoms separated by 2.5 Å (21). Electrons from cytochrome *c* enter CcO at the Cu_A site and are further transferred via heme *a* to heme a_3 and Cu_B. Protons from the cytoplasm enter the enzyme via the D- or K-proton pathways (10–13, 22, 23). These pathways connect the aqueous cytoplasmic phase with the conserved Glu-278[3] in the interior of the enzyme (D-pathway) or with the binuclear center (K-pathway). The proton exit route to the periplasm is less well defined. Water is expelled to the periplasm via the Mg^{2+} or Mn^{2+} bound at the interface of subunits I and II (24–27).

The oxygen-reduction cycle of CcO has been studied by a great variety of kinetic techniques such as the flow-flash method monitored by UV-visible spectroscopy (10–13, 23,

* This work was supported by the Foundation for Fundamental Research on Matter (FOM) (Grant FOM-D26) and the Deutsche Forschungsgemeinschaft (Grant SFB 472). The costs of publication of this article were defrayed in part by the payment of page charges. This article must therefore be hereby marked "*advertisement*" in accordance with 18 U.S.C. Section 1734 solely to indicate this fact.

[S] The on-line version of this article (available at http://www.jbc.org) contains supplemental Figs. S1–S3 and Table S1.

[1] To whom correspondence should be addressed. Tel.: 31-152-785-139; Fax: 31-152-782-355; E-mail: s.devries@tudelft.nl.

[2] The abbreviations used are: CcO, cytochrome *c* oxidase; MHQ, microsecond freeze-hyperquenching; Trp*, tryptophan radical; Trp-272*, the neutral radical of Trp-272.

[3] The residue numbering refers to the *P. denitrificans* aa_3 cytochrome *c* oxidase sequence.

This is an Open Access article under the CC BY license.

28–31) or resonance Raman scattering (32–38). Collectively these studies have led to a general understanding of the catalytic mechanism in terms of oxygen chemistry, electron transfer, and proton translocation. The catalytic cycle can be initiated from the fully reduced enzyme (*R*) or from the mixed-valence form (*MV*) in which only heme a_3 and Cu_B are reduced or by single electron injection (11, 39).

When the reaction is started with the fully reduced CcO, the enzyme cycles through a series of intermediates designated as $R \rightarrow A \rightarrow P_M \rightarrow P_R \rightarrow F \rightarrow O_H$ (see Fig. 7 below). The first detectable intermediate after mixing *R* with O_2, *A*, is formed within ~10 μs. *A* is the oxy-ferrous complex (Fe^{2+}–O_2) of heme a_3 (29–31, 34–38). Subsequently, the O=O bond is broken yielding P_M. P_M accumulates (~150 μs) when the reaction is started with *MV*. However, when the reaction is initiated from *R*, P_R accumulates (completed in ~100 μs). Direct evidence for O=O bond splitting in both P_M and P_R was provided by resonance Raman spectroscopy, which identified the specific vibrations of the oxoferryl (Fe^{4+}=O) state of heme a_3 (34–38). In P_M and P_R, the Cu_B^{1+} has been oxidized to Cu_B^{2+}–OH^-. The oxygen atom in Cu_B^{2+}–OH^- is derived from molecular oxygen (40). The breaking of the O=O bond requires donation of four electrons and a proton. Because this also occurs when the reaction is started with *MV*, whereas heme a_3 and Cu_B provide only three electrons, an amino acid, Tyr-280 (*P. denitrificans* numbering), was proposed to act as the donor of the fourth electron (plus the proton) (33). Tyr-280 is covalently linked to His-276, a ligand to Cu_B, and sufficiently close to the binuclear center to act as a rapid reductant (8, 14, 16–18). Indeed, some Tyr-280 had been converted to the radical Tyr-280* in P_M (41). In P_R, in contrast to P_M, the Tyr-280* is absent (42) presumably because it has been reduced by heme *a* to the anion (Tyr-280^-) or to the protonated Tyr-280. Even though heme *a* oxidation in the sequence $R \rightarrow A \rightarrow P_M \rightarrow P_R$ is completed within ~100 μs, the true rate of electron transfer from heme *a* to heme a_3 (and to Tyr-280*?) is ~1 ns (43), which would explain why P_M (and Tyr-280*) does (do) not accumulate to a measurable extent when the reaction is started from *R*. Instead of Tyr-280, the conserved Trp-272 has been proposed recently as the amino acid residue involved in O=O bond breaking (44).

The $P_R \rightarrow F$ transition is not associated with electron transfer but with proton binding and proton translocation (9–13). The slowest step of the oxidative part of the catalytic cycle (1–1.5 ms) is the $F \rightarrow O_H$ transition, which is linked to proton translocation as well (9–13). In this step an electron is transferred from Cu_A/heme *a* to Fe^{4+}=O yielding Fe^{3+}–OH^- (38). At this stage, the enzyme is completely oxidized, but in a metastable "high energy state," O_H. Reduction of O_H, but not of the resting enzyme (*O*), leads to two successive proton-pumping events in the reaction sequence $O_H \rightarrow E \rightarrow MV$ (11, 45).

To resolve enzyme catalytic mechanisms on the microsecond time scale, we have developed a microsecond freeze-hyperquenching mixing/sampling device (MHQ) (5, 46–48). MHQ is an extension of the rapid-freeze quench technique (49) in which the instrument dead time has been reduced from 5–7 ms to 60–80 μs (46, 47). The great advantage of MHQ and rapid-freeze quench is that the resulting frozen powder containing trapped intermediates can be analyzed by a variety of spectroscopic techniques, including EPR spectroscopy, an invaluable tool in the study of metallo-redox enzymes. MHQ experiments with cytochrome bo_3 from *Escherichia coli* and cytochrome aa_3 from *P. denitrificans* showed the formation of a tryptophan radical (Trp*) after ~200 μs, which was weakly magnetically coupled to the Fe^{4+}=O state of the heme a_3 (46). The EPR properties of this transient radical differ from the Tyr-167* and the proposed porphyrin cation and/or tryptophan radicals obtained by incubation with H_2O_2 (50–52).

In the work presented in this report we used MHQ to determine the kinetics of the Trp* found previously and assign its role in the catalytic cycle. Q-band EPR spectroscopy identifies the radical as the neutral radical form of Trp-272. The kinetics of Trp-272*, Cu_A, heme *a*, and heme a_3 were determined and simulated with a single set of rate constants in a model including the new intermediate F_W*, which harbors the Trp-272*. The Trp-272* is formed in the second part of the catalytic cycle and Trp-272 is proposed as the electron donor to heme a_3 or Cu_B. An additional role for Trp-272 in proton pumping is discussed.

EXPERIMENTAL PROCEDURES

Enzyme Purification—P. denitrificans cytochrome aa_3 was purified as previously described (53, 54) and contained 0.2 mol Mn^{2+} per mole of enzyme as determined by EPR spectroscopy. Mn^{2+}-depleted enzyme was obtained by decreasing the Mn^{2+} concentration to 0.5 μM in the growth medium (55, 56).

Microsecond Freeze-hyperquenching and Sample Handling—The MHQ setup (dead time of 60 - 80 μs and effective reaction temperature of 10 ± 1 °C.) and the sample handling procedures are identical to those described before (5, 46) except that the aluminum rotating cold plate was coated with a layer of ~5 μm of 99.999+ % tungsten. Tungsten was applied in 50 cycles of physical vapor deposition. The tungsten coating of the cold plate resulted in lower impurities (*e.g.* Fe^{3+} trapped in corundum) in the samples analyzed by EPR spectroscopy. For each time point 0.25 ml of pulsed cytochrome aa_3 (100–280 μM) was used (5, 46). The reduced enzyme (incubated with 10 mM ascorbate and 1 μM phenazine ethosulfate) was mixed 1:1 with an O_2-saturated (1.3 mM at 20 °C) buffer (50 mM HEPES, pH 7.2, 0.1% laurylmaltoside). Sample preparation for the low temperature UV-visible spectroscopy and normalization and analysis of the spectra are described in (46). Sample packing is described previously (47).

UV-visible Spectroscopy—UV-visible spectra were recorded with an Olis upgraded Aminco DW2000 scanning spectrophotometer equipped with a custom-made liquid N_2-flow system, to maintain the temperature during the measurement stable at 90 K (48). The spectrophotometer was calibrated with a holmium oxide filter to an accuracy of 0.2 nm.

Data Analysis—Data were processed and analyzed with the IGOR Pro software package (Wavemetrics). Q-band EPR spectra were simulated using a home-written simulation program in Pascal for the Macintosh computer. The program allows for non-linear g- and A-tensors. The kinetic data were fitted to a model of six consecutive irreversible reactions. The analytical solution of this set of homogeneous first-order differential equations has been added to the supplemental information.

EPR Spectroscopy—X-band EPR spectroscopy was performed on a Bruker ER200D spectrometer, Q-band EPR spectra were recorded on a Varian E9 spectrometer. Both spectrometers were equipped with a home-built helium-flow system (57). EPR signals were quantitated with respect to a 10 mM $CuClO_4$ standard. Differences in sample packing were corrected using the Mn^{2+} signal as internal standard in case Mn^{2+}-containing CcO was used (see supplemental Fig. S2). For Mn^{2+}-free CcO no correction for sample packing was applied, only for differences in starting concentrations of the CcO. The overall dilution of the enzyme as present in the EPR tube is 6- to 10-fold with respect to the starting concentration. This dilution arises from the 1:1 mixing, condensation of water vapor during sample handling, and the loose sample packing owing to the fine nature of the frozen powder. The uncertainty in sample packing was determined at 1 ± 0.20 ($n = 25$) and is indicated with *error bars* in the figures. However, the relative concentrations of Cu_A, heme *a* and the Trp* are accurate to 1 ± 0.05, because they are determined in the same sample. The *g* values of the Trp* at Q-band frequency were determined with 2,2-diphenyl-1-picrylhydrazyl and the Mn^{2+} signal as an internal standard and are accurate to ± 0.0002.

RESULTS

Low Temperature UV-visible Spectroscopy of MHQ Samples—MHQ samples were prepared by reacting fully reduced cytochrome aa_3 with O_2 for various times between 83 μs and 6 ms. Fig. 1 shows the low temperature absolute and difference UV-visible spectra of a selection of these samples. In the first 130 μs of the reaction the absorbance of the Soret band at 444 nm decreased, and a new band appears at 430 nm (Fig. 1*A*). The difference spectra (Fig. 1*B*) indicate a loss of intensity of ~50% at 444 nm. Concomitantly, the α-band shifted from 603 to 606 nm (Fig. 1*A*) or, in the difference spectra (Fig. 1*B*), to 608 nm while losing some intensity. The peaks at 430 and 606 nm in the absolute spectra are characteristic for the oxoferryl state ($Fe^{4+}=O$) of heme a_3, and the P-state, specifically P_R (32–38). The spectra obtained after 220 and 355 μs indicated a small blue shift of the α-band from 608 to 603–604 nm without a change in the Soret region (Fig. 1*B*). This blue shift is consistent with the $P_R \rightarrow F$ transition (10–13, 23, 28–31, 33, 35, 38). More direct evidence for the formation of *F* came from control experiments using H_2O_2 (data not shown) to generate *F* at pH 6 and 7.2, the latter being the pH in our experiments. These experiments were performed exactly as in a previous study (44). Samples were first monitored at room temperature to check for formation of *F* and subsequently frozen for analysis at 90 K by UV-visible spectroscopy. The low temperature UV-visible difference spectra (H_2O_2 minus oxidized enzyme) indicated the formation of a broad band with a maximum at 571 ± 1 nm instead of 580 nm at room temperature (42, 44, 58, 59). The amplitude of the 571 nm band amounted to 7 and 11% (at pH 7.2 and 6, respectively) of the α-band intensity of the absolute spectrum of oxidized enzyme (compare with Ref. 59). Fig. 1*B* shows a shift in the β-band position from 565 nm at $t = 0$ to 571 nm indicating formation of *F*. The 571 nm maximum persisted up to 3 ms, which suggests rapid formation and relatively slow breakdown (1–1.5 ms) of *F*. The kinetics of formation and

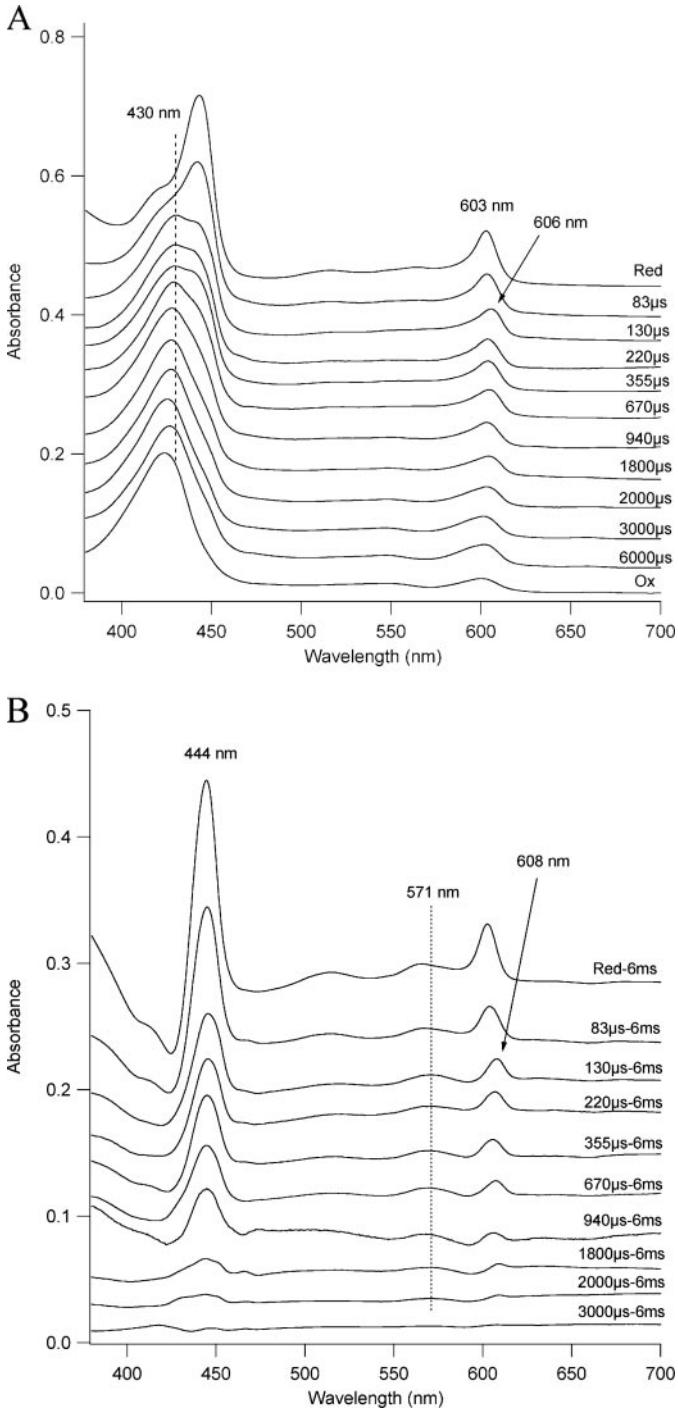

FIGURE 1. **Low temperature absolute (*A*) and difference (*B*) visible spectra of cytochrome aa_3 from *P. denitrificans* recorded at 90 K.** Fully reduced pulsed cytochrome aa_3 was rapidly mixed with an O_2-saturated buffer and reacted for various times (indicated in microseconds). "*Red*" refers to fully reduced cytochrome aa_3 with maxima at 444 nm in the Soret region and at 603 nm in the α-band region. *A*, the Soret maximum of the oxoferryl form of heme a_3 is at 430 nm. Formation of P_R (606 nm) after 130 μs is indicated by an *arrow*. The peak shifts to 603/604 nm after 220 μs and longer times. After 6 ms the enzyme is oxidized (O_H); the Soret maximum is 427 nm. "*Ox*" refers to the as-isolated oxidized form of cytochrome aa_3 displaying maxima at 424 nm and 600 nm in the Soret and α-band regions, respectively. *B*, the spectrum obtained after 6 ms was subtracted from those in *A*. The Soret maximum of reduced hemes ($a + a_3$) is 444 nm. Formation of P_R (608 nm) after 130 μs is indicated by an *arrow*. The peak shifts to 603/604 nm after 220 μs and longer times. Formation of *F* is indicated by the shift of the β-band from 565 nm to 571 nm (0–130 μs). Decay of *F* is seen as a decrease in intensity of the 571 nm band (355 μs to 3000 μs).

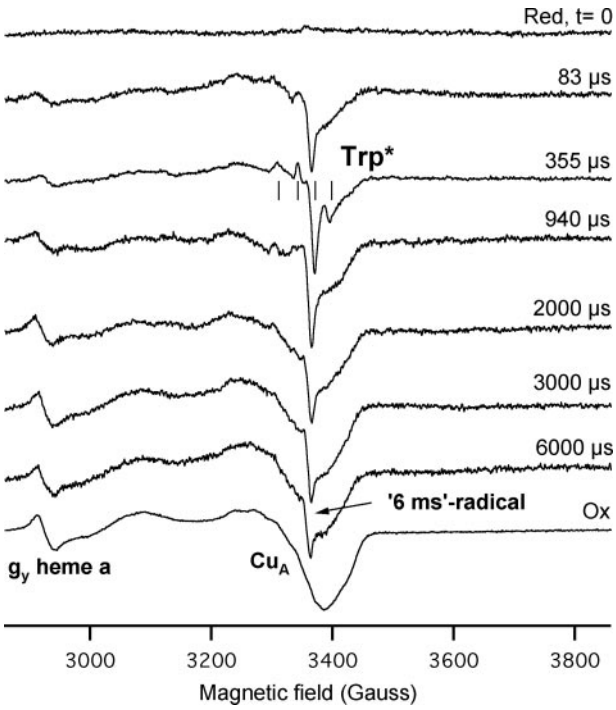

FIGURE 2. **Representative X-band EPR spectra of cytochrome *aa*$_3$ from *P. denitrificans* rapidly mixed with O_2 and reacted for various times (indicated in microseconds).** The four *vertical lines* indicate the peaks of the Trp* (spectrum after 355 μs). The g_y resonance of heme *a* and the $g_\perp$ of Cu_A were used to determine their redox states. EPR conditions: frequency, 9.42 GHz; modulation amplitude, 1.0 millitesla; microwave power, 2 milliwatts; temperature, 14 K. The spectra are normalized correcting for differences in gain and enzyme concentrations.

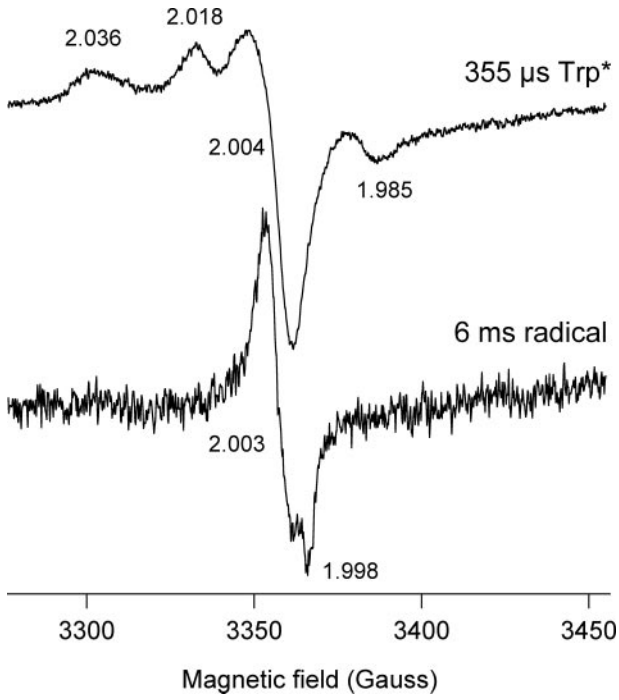

FIGURE 3. **X-band EPR spectra showing two different radicals formed by cytochrome *aa*$_3$ from *P. denitrificans* during the reaction cycle.** The enzyme has reacted for 355 μs (Trp*) or 6 ms (*lower spectrum*). The apparent *g* values are indicated. EPR conditions: frequency, 9.411 GHz; modulation amplitude, 0.5 millitesla; microwave power, 0.2 milliwatt; temperature, 14 K. Each spectrum is an average of four. The spectrum of the 6-ms radical was expanded vertically five times with respect to the 355-μs Trp* spectrum. The starting CcO concentrations were 280 μM (355 μs) and 120 μM.

breakdown of *F* were calculated from Fig. 1*B* (see Fig. 8) and are in good agreement with the data in Refs. 28 and 38.

After the formation of *F* the Soret maximum at 430 nm shifts to 427 nm (completed after 3–6 ms), corresponding to the absorbance maximum of the oxidized (pulsed) enzyme (Fig. 1*A*). The disappearance of the Soret maximum at 444 nm also points to complete oxidation of hemes ($a + a_3$) after 3–6 ms (Fig. 1*B*). The UV-visible spectra did not resolve the concomitant reduction of heme a_3 (Fe^{4+}=O to Fe^{3+}–OH^-) and oxidation of heme *a*, neither in the Soret region nor in the α-band. The intensity of the α-band decreased (355 μs to 6 ms) due to oxidation of heme *a*. Control stopped-flow experiments indicated that after 4–6 ms no further optical changes occurred up to several minutes (data not shown).

When the oxidation of the hemes ($a + a_3$) was calculated as the optical absorbance difference at 444–462 nm (supplemental Fig. S1), the characteristic apparent biphasic oxidation was observed, similar to that for the bovine heart mitochondrial cytochrome *aa*$_3$ oxidase (28).

EPR Spectroscopy of MHQ Samples—Representative EPR spectra of the Mn^{2+}-free CcO samples are shown in Fig. 2. The magnetic field range displayed is suitable for the determination of the redox states of heme *a*, Cu_A, Cu_B, and for the detection of the radical described previously (5, 46). The figure shows rapid oxidation of heme *a* and Cu_A to ~50% after 83 μs and 355 μs, whereas the remainder was oxidized on the millisecond time scale. The Trp* was developed maximally after 355 μs and disappeared within a few milliseconds concomitant with the second slow heme a/Cu_A oxidation phase (Fig. 2). After 6 ms another radical was observed, called the "6-ms radical" (Fig. 3).

The X-band EPR spectrum of the Trp* (355 μs) in Mn^{2+}-depleted CcO (Fig. 3) was slightly of a different form than that reported previously; in that work the contribution from Mn^{2+} had to be subtracted (see Fig. 2 in Ref. 46). In particular, the low field line ($g = 1.985$) was poorly resolved but present in both the cytochrome *aa*$_3$ and cytochrome *bo*$_3$ EPR spectra. The Trp* X-band EPR signal consists of four lines with apparent *g* values of $g = 2.036$, 2.018, 2.004, and 1.985. We have previously attributed the lines at $g = 2.036$ and $g = 2.004$ to a Trp* weakly magnetically coupled ($J_{x,y} = -4.9$ GHz) to the heme a_3 Fe^{4+}=O state (46). The lines at $g = 2.018$ and $g = 2.005$ could originate from a second Trp* (with $J_{x,y} = -2.1$ GHz) or from a Tyr* also including a low field feature now clearly resolved at $g = 1.985$. Q-band EPR spectroscopy (Fig. 4) leads to a revision of this assignment regarding the Tyr*.

The EPR line shape of the four-line radical signal is fairly constant in the MHQ samples obtained up to 940 μs. However, after 2 ms and longer reaction times, a sharp and at X-band frequency axial signal with $g_\perp = 2.003$ and $g_\parallel = 1.998$ had clearly developed, which is the 6-ms radical spectrally overlapping with the Trp* (Figs. 2 and 3). In particular, part of the sharp feature at $g = 2.004$ of the Trp* is due to a contribution of the 6-ms radical (Fig. 3).

EPR spectroscopy of the 355-μs and 6-ms MHQ samples at Q-band frequency allowed a more solid assignment of the radical (Fig. 4). The four-line spectrum of the Trp* at X-band from $g = 2.04$ to $g = 1.98$ is apparently confined to a narrow magnetic

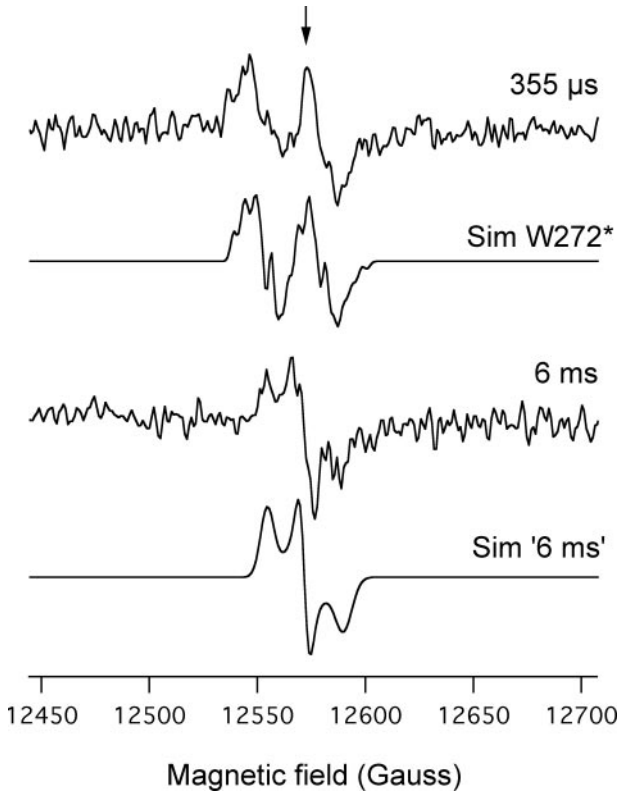

FIGURE 4. **Q-band EPR spectra of the Trp* (355 μs), the 6-ms radical, and their simulations.** Part of the MHQ frozen powder used for the samples of Fig. 4 was transferred to Q-band EPR tubes. The 6-ms radical contributes slightly to the Trp* in the spectrum of the 355-μs sample. This is seen most clearly in the *positive part* of the *right line*, which is relatively sharp. In this region (indicated by an *arrow*) the fit to the experimental spectrum is somewhat less. The simulation parameters for the Trp* are listed in Table 1. Those for the 6-ms radical are: $g_{x,y,z}$ = 2.0022, 1.9965, and 1.9994. EPR conditions: frequency, 34.972 GHz; modulation amplitude, 1.0 millitesla; microwave power, 2.5 and 5 milliwatts (6-ms sample); temperature, 16 K. Each spectrum is an average of 85 scans.

field region around $g = 2$. The Zeeman interaction at Q-band frequency (35 GHz) is now much larger than the weak magnetic dipolar/exchange coupling (−4.9 GHz) leading to a simplification of the four-line spectrum seen at X-band frequencies. The Q-band spectrum of the 6-ms radical (Fig. 4) was better resolved than the X-band spectrum (Fig. 3) displaying a three-line rhombic signal. The rhombic signal represents ~0.5% of the CcO concentration. The 6-ms radical is not an ascorbate or PES radical. The absence of resolved hyperfine structure in its spectrum and the *g* values ($g_{x,y,z}$ = 2.0022, 1.9965, and 1.9994) close to the free electron *g* value suggested an organic radical, perhaps a main-chain radical. The structural characterization and the possible function of this radical must await further experimentation.

The Q-band EPR spectrum of the radical obtained after 355 μs can be simulated as an $S = ½$ system with simulation parameters (Table 1) characteristic for Trp* radicals (60–62), in agreement with our previous assignment (46). The hyperfine constants determined by the simulation can be used to calculate the dihedral angles of the β-methylene protons with respect to the indole ring (60–62). Because the dihedral angles are known from the crystal structure (8, 14, 16–18), the radical was assigned as residing at Trp-272 (see Table 1 and "Discussion"). Tyrosine radicals have much larger *g*-anisotropy (56, 62–65) and are absent from the spectrum. The Trp-272* EPR spectrum contained a small contribution from the 6-ms radical (indicated by the *arrow* in Fig. 4), which was not reproduced in the simulation of Trp-272*.

The kinetics of the Trp-272* calculated from the X-band EPR spectra is displayed in Fig. 5. The maximum amount of the Trp-272* was formed after 300–500 μs and amounted to 4–5% of the CcO. The transient was fitted with the same rate constants as the Cu_A and heme *a* traces (Fig. 6) and apply to the model shown in Fig. 7. The relatively slow formation of the

TABLE 1

Orientation of the β-methylene protons of Trp residues of *P. denitrifcans* CcO conserved in Type A1 oxidases, their predicted hyperfine ratios ($H\beta_2/H\beta_1$), and the simulation parameters for the Trp*

Residue	Dihedral angle		$H\beta_2/H\beta_1$	Distance[a]			Comment
	θ_1	θ_2		δa_3-C_3	δCu_B-C_3	δa-C_3	
	°				Å		
Trp-164	−13.6	−133.6	0.503	8.5	5.3	11.9	Trp* in W164T
Trp-272	3.8	123.8	0.31	9.8	7.1	13.4	O.k.
Trp-323	30.9	150.9	1.04	10.7	7.5	18.0	Wrong $H\beta_2/H\beta_1$
Trp-358	−81.5	158.5	0.025	16.1	21.9	22.2	*F* in *A. pernix*
Trp-375[b]	−3.8	116.2	0.196	18.6	25.4	15.6	Too far[d]
Trp-431[c]	−78.5	161.5	0.044	23.5	29.5	22.2	Too far[d]
Trp-532	−2.8	118.2	0.22	28.8	34.6	29.2	Too far[d]
Trp-136	−10.7	109.3	0.113	29.2	31.3	24.7	Too far[d]
Trp-22	4.9	124.9	0.33	34.1	37.1	27.5	Too far[d]
Experimental	θ_1, 3.1	θ_2, 123.1	$H\beta_2/H\beta_1$, 0.30				
S.D.[e]			0–0.4				
Simulation parameters	*g*	$H\beta_1$ (Gauss)	$H\beta_2$ (Gauss)	H5 (Gauss)	H7 (Gauss)	N (Gauss)	
xx	2.0035	25	7.5	7	0	0	
yy	2.0026	25	7.5	0	5	0	
zz	2.0023	25	7.5	5	5	9	

[a] δa_3-C_3, δCu_B-C_3, and δCa-C_3: shortest distance from the C3 atom of the respective tryptophan residue to heme a_3, Cu_B, *and heme a*, respectively. About 50% of the spin density is located at the C3 atom.

[b] Not conserved in other oxidases.

[c] *Y* in *S. acidocaldarius*.

[d] The dihedral angles θ_1 and θ_2 are calculated from the crystal structure of *P. denitrificans* CcO (PDB entry 1QLE). The dipolar/exchange coupling of the oxoferryl-Trp-119 radical in cytochrome *c* peroxidase (−4.9 GHz) is the same as that observed for the Trp-272*. The coupling of −4.9 GHz yields for both radicals a peak at $g_z \sim 2.04$. The Trp* and Tyr* described in Refs. 61–65 with similar couplings/g_z-values are all located within 9 Å from the oxoferryl. The dipolar contribution to the magnetic coupling is dominant over the exchange coupling at distances >3–4 Å and falls off with the third power of the distance. Trp-358, at 16.1 Å, is expected to yield a coupling of <1 GHz or $g_z \sim 2.009$, which is not seen in the X-band EPR spectrum. Both Trp-164 and Trp-272 are at distances from the oxoferryl consistent with the $g_z \sim 2.04$.

[e] "Standard deviation," the value for the ratio $H\beta_2/H\beta_1$ yielding EPR spectra quite similar to the experimental spectrum. See supplemental Fig. S3 and text for further explanation.

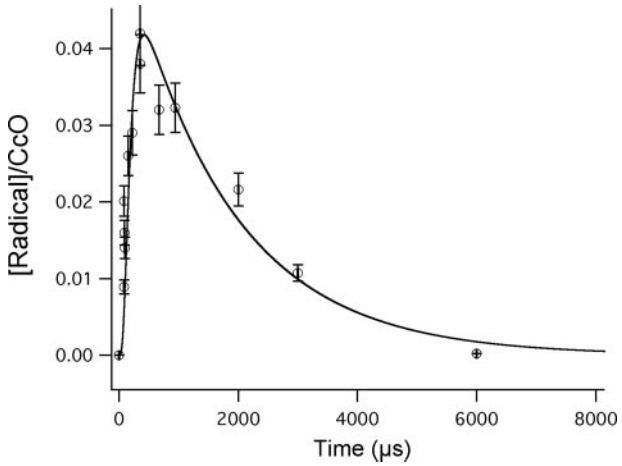

FIGURE 5. **Time course of the tryptophan radical.** The amount of radical (*open circles*) was determined from the X-band EPR spectra taken from freeze-quenched samples. The *line* through the data points is a simulation using the rate constants of Fig. 7 and represents the kinetics of F_W* (Fig. 8), indicating an apparent half-life of formation of 157 μs, maximal Trp* level after 414 μs, and an apparent half-life of breakdown of 1.71 ms, yielding 0.042 Trp*/CcO as the maximal amount of radical formed. Note that, when species accumulate to low amounts like the Trp*, the apparent rate of formation is actually closer to the rate of decay and *vice versa* (76).

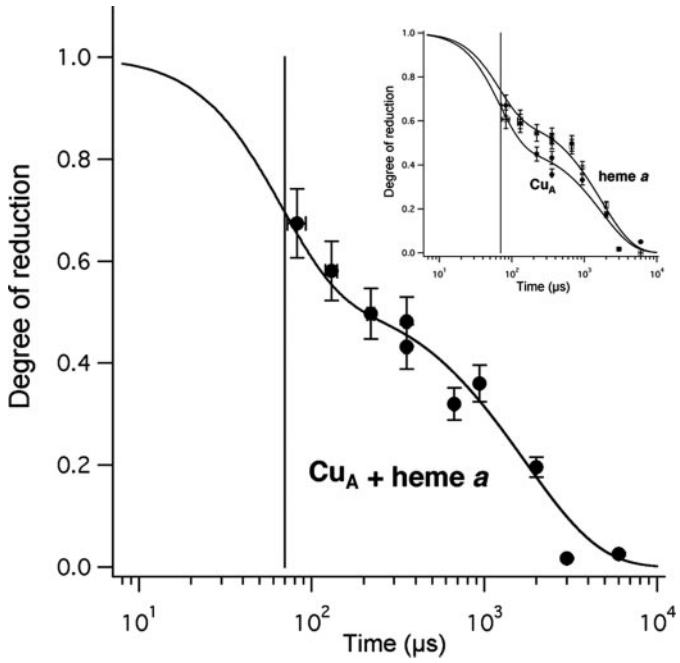

FIGURE 6. **Oxidation kinetics of (Cu_A + heme *a*) (*filled circles*) and in the inset of Cu_A (*filled circles*) and heme *a* (*open circles*) plotted separately.** Redox states of heme *a* and Cu_A were calculated from EPR spectra as shown in Fig. 2. The *lines* through the data are simulations using the six rate constants shown in the model of Fig. 7 and further applying the K_{eq} = 1.2 for the Cu_A/heme *a* equilibrium to calculate the traces of the *inset*. A single electron is donated by (Cu_A + heme *a*) in each oxidation phase. The *vertical line* represents the MHQ dead time (60–80 μs), positioned at 70 μs.

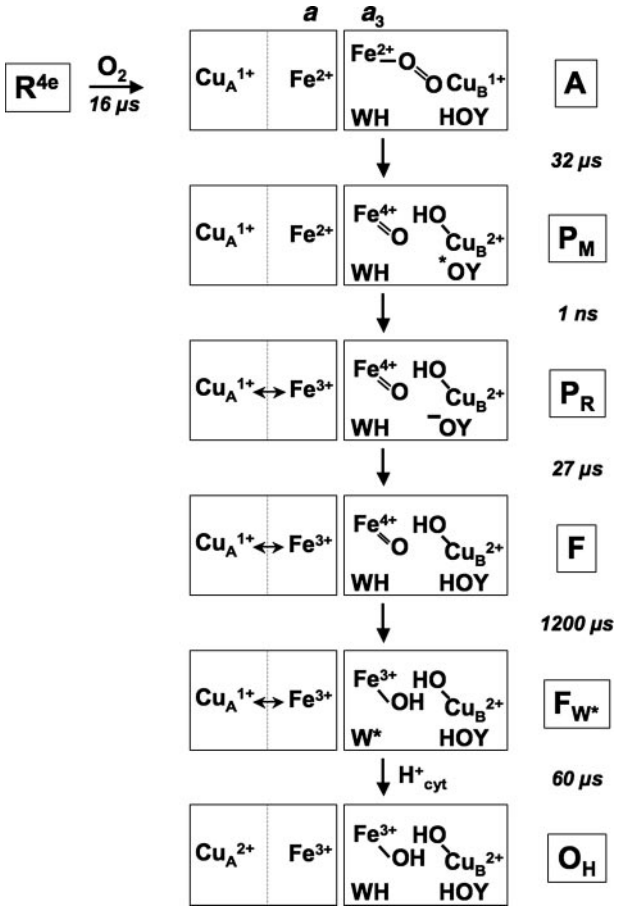

FIGURE 7. **Reaction scheme of CcO showing the various intermediates with their half-lives.** *WH*, Trp-272; *W**, Trp-272*. Pumped and chemical protons are largely omitted from the scheme for reasons of clarity, except "H^+_{cyt}" for the F_W* → O_H transition. Likewise, formation of the Trp-272$^-$ anion is not shown explicitly; the anion is formed in the F_W* → O_H transition by electron transfer from Cu_A/heme *a* prior to protonation to Trp-272 by "H^+_{cyt}". "H^+_{cyt}" signifies a proton originating from the cytoplasm that has traveled along one of the proton pathways. The direct proton donor to the Trp-272$^-$ anion might be *e.g.* Glu-278, a heme propionic acid residue, or an active site water molecule (see text for further details). *HOY*, **OY*, and $^-$*OY* refer to Tyr-280, its radical, and anion forms, respectively. Instead of Tyr-280, Trp-272 might be involved in the sequence P_M → *F* (see text). The half-lives shown in the scheme were derived as follows: *R* → *A*: calculated from Ref. 29 for 0.65 mM O_2. *A* → P_M: imposed by simulation of the (initial phase of) Cu_A/heme *a* and Trp* radical kinetics and in agreement with previous studies (28, 38, 68, 69). P_M → P_R: taken from Ref. 43. P_R → F: calculated from the simulation of the formation/decay of *F* (Fig. 1*B*) and the Cu_A/heme *a* and Trp* radical kinetics. *F* → F_W* and F_W* → O_H: calculated from the (second phase of) Cu_A/heme *a* oxidation and Trp-272* transient kinetics. The half-lives of 1200 μs and 60 μs model the Trp-272* transient kinetics and its accumulation to 4.2%. The half-life of 60 μs is due to electron transfer from Cu_A/heme *a* to the Trp-272*. See text for further explanation.

Trp-272* (1200 μs) and its rapid breakdown (60 μs) are consistent with the total accumulation to 4–5% as determined by EPR.

The oxidation kinetics of Cu_A and heme *a* determined by EPR are presented in Fig. 6. Cu_A and heme *a* are oxidized in two kinetic phases. The kinetics of Cu_A and heme *a* suggest very similar reduction potentials for the two cofactors. The calculated equilibrium constant, K_{eq} = 1.20 ± 0.23, corresponds to a 4.5 ± 5.4 mV (n = 9) lower midpoint potential for Cu_A relative to heme *a* (Fig. 6, *inset*), a value in good agreement with pulse radiolysis experiments monitored optically (66). Assuming redox equilibrium, the slightly lower midpoint potential of Cu_A led to the slightly higher *apparent* rate of oxidation of Cu_A (apparent $t_{1/2}$ = 50 μs for 25% oxidation) relative to heme *a* (apparent $t_{1/2}$ = 65 μs for 25% oxidation) (Fig. 6, *inset*). The apparent half-lives for the second phase (each component oxidized for 75%) were 1.22 and 1.62 ms for Cu_A and heme *a*, respectively. Fig. 6 further shows that Cu_A plus heme *a* acts as a redox pair donating a

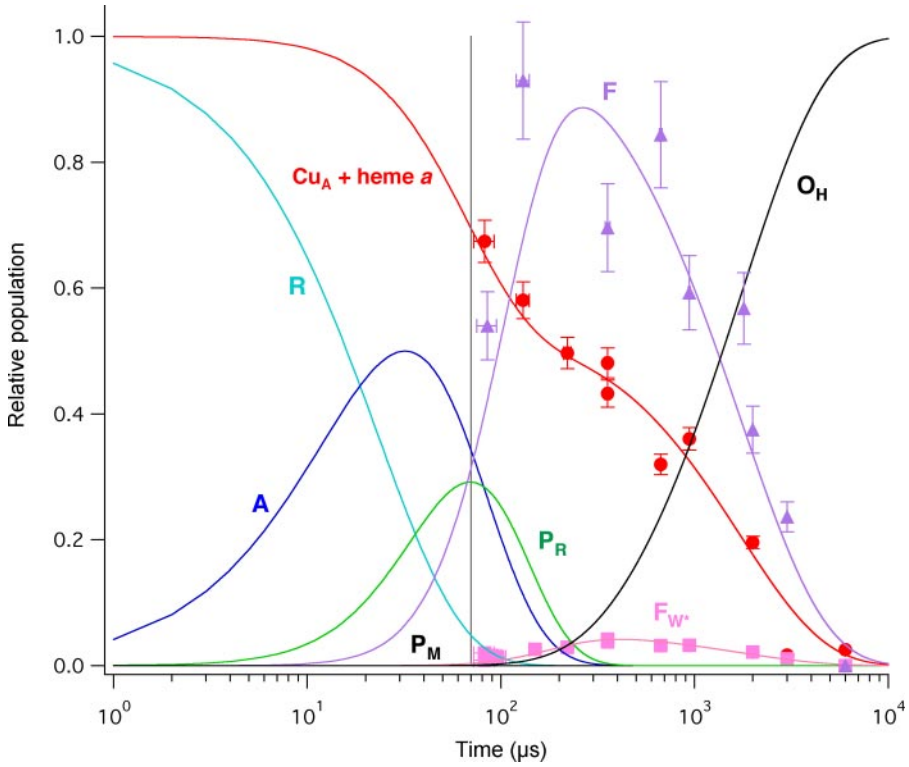

FIGURE 8. **Simulated populations of the various intermediates formed in a single turnover of fully reduced cytochrome oxidase reacting with O_2.** Simulations reflect a single set of half-lives based on the experimental data for the oxidation of Cu_A and heme *a*, *F*, and Trp-272* (F_W*). Experimental data for formation of O_H, which can be calculated directly from the relative populations of *F*, F_W*, and the redox state of Cu_A/heme *a*, are omitted from the figure. The analytical solutions for the formation of the intermediates and the calculation of the redox state of Cu_A and heme *a* are given in the supplemental material. The calculated populations of *A*, which could not be resolved experimentally, and of P_R, which was observed (Fig. 1*B*), were calculated as indicated in the legend to Fig. 7 and are in excellent agreement with previous studies (28, 38, 68, 69). Note that the intermediate P_M does not accumulate, due to its rapid (1 ns) conversion to P_R. The *vertical line* represents the MHQ dead time (60–80 μs), positioned at 70 μs. The *symbols* are experimentally determined values. *Squares*, Trp-272* (and F_W*); *circles*, Cu_A plus heme *a*; *triangles*, *F*. *F* was measured at 571 nm (*cf.* Fig. 1*B*).

single electron to the binuclear center in each oxidation phase.

The typical four-line EPR signal of Cu_B (40, 42) was not detected in any of the MHQ samples, even though the temperature was varied between 6 and 100 K, and the microwave power was between 20 microwatts and 200 milliwatts. All samples including the time-zero sample, showed the $g = 6$ a signal of Fe^{3+} high-spin heme a_3, but its intensity was low (<3% of the CcO) and hardly changed (though slightly increased) between $t = 0$ and 6 ms (data not shown). These $g = 6$ data were not further analyzed.

The EPR spectra of MHQ samples obtained with Mn^{2+}-containing enzyme are shown in supplemental Fig. S2. For these samples quantitation of the radical intensity and Cu_A was more difficult due to overlap of the Mn^{2+} EPR spectrum. However, the Mn^{2+} signal served as a good internal standard to determine sample reproducibility even though the Mn^{2+} spectrum is dependent on the redox state of Cu_A (27). The sample preparation reproducibility ($n = 25$) was determined at 1 ± 0.20. The kinetic behavior of Mn^{2+}-containing or Mn^{2+}-depleted cytochrome aa_3 was found to be indistinguishable, consistent with similar turnover numbers (180–190 O_2 s^{-1}) for both types of oxidase preparations. Therefore, Figs. 1, 5, 6, 8, and S1 display data obtained for both types of enzymes.

DISCUSSION

In the oxidative part of the catalytic cycle of *P. denitrificans* cytochrome aa_3 two radicals are formed as determined by MHQ in conjunction with X-band and Q-band EPR spectroscopy. Simulation of the Q-band EPR spectrum identifies one of the radicals as the catalytically competent tryptophan-neutral radical of the strictly conserved Trp-272 (Trp-272*). Formation of Trp-272* constitutes the rate-limiting step of the catalytic cycle. The current finding that the Trp-272 radical is neutral demonstrates that this residue couples electron transfer to proton movements. We will discuss below how oxidoreduction of Trp-272 can provide the driving force for the transmembrane movement of protons ("proton pumping") through its participation in a proton-relay network. Our findings underscore the general importance of amino acid side chains in coupling electron transfer to proton transfer reactions, alongside the well known metallo-redox centers.

In this report a full kinetic profile in a time window of 83 μs to 6 ms has been determined for the oxidation-reduction kinetics of Cu_A, heme *a*, heme a_3, and the Trp-272*. EPR spectroscopy has the great advantage over UV-visible and resonance Raman spectroscopy in that the concentrations of these components can be determined without mutual spectral interference and without assumptions about the (relative) extinction coefficients or the resonance enhancement. The assignment of the Trp-272* and its possible function in catalysis are discussed within the framework of the model presented in Fig. 7. This model describes the oxidation route of the fully reduced enzyme by the reaction sequence $R \rightarrow A \rightarrow P_M \rightarrow P_R \rightarrow F \rightarrow F_W^* \rightarrow O_H$ in which the new intermediate F_W^* contains the Trp-272*. Simulations of the kinetic traces (Figs. 5 and 6) were performed with a *single* set of rate constants (half-lives) shown in Fig. 7. The appearance and accumulation of the various intermediates is depicted in Fig. 8.

Scope and Limitations of the MHQ Setup—The formation of *A* ($t_{½}$ = 16 μs at 0.65 mM O_2 (29)) could not be resolved, because the instrumental dead time of the MHQ setup is 60–80 μs. The oxygen-binding rate has been established with the flow-flash setup monitored by UV-visible spectroscopy (dead time ~ 1.5 μs determined by the CO dissociation rate (29)), and the structural assignment of *A* (Fe^{2+}–O_2) is based on resonance Raman

spectroscopy (dead time ~25 μs (32–38)). We did observe the formation of P_R ($Fe^{4+}=O$) indicated by the α-band absorbance shift to 606 nm (608 nm in the difference spectra) concomitant with the formation of the Soret absorbance at 430 nm and the disappearance of ~50% of the Soret intensity at 444 nm (Fig. 1 and supplemental Fig. S1). The formation of *F* at 571 nm was also detected. In addition we could resolve and analyze by EPR spectroscopy rather than by UV-visible spectroscopy part of the initial oxidation phase of heme *a* and Cu_A. Transfer of the first electron to the binuclear center after O=O bond splitting was completed in ~130/200 μs (Figs. 6–8).

The heme ($a + a_3$) oxidation kinetics follow the characteristic biphasic pattern of the fully reduced enzyme (supplemental Fig. S1 (28)). In our work the UV-visible spectral data were obtained from independently frozen samples, in contrast to the "continuous" flow-flash methods, and have to be normalized to compare the redox states of the hemes between different samples (5, 46, 48). Because our data could be simulated with a similar set of kinetic and spectral parameters as for the bovine heart enzyme (Ref. 28 and supplemental Fig. S1), we conclude that the normalization procedure is adequate. A multicomponent analysis of the UV-visible spectra to determine the spectra of the intermediates *A*, P_R, or *F* proved too difficult at present and has not been pursued.

Formation of P_R, F, and O_H—The major intermediate accumulating to 80–90% after 200–400 μs is *F* (28, 35, 36, 38), formed by rapid protonation of P_R (Figs. 7 and 8). Although the optical spectra of P_R and *F* were indistinguishable in the Soret region (maximum at 430 nm due to $Fe^{4+}=O$ of heme a_3), *F* absorbed at 571 nm in the low temperature UV-visible spectrum and P_R at 608 nm (606 nm in the absolute spectrum). We could monitor the shift in the α-band to 608 (606) nm (at 130 μs, Fig. 1, *A* and *B*) signifying P_R formation, and at slightly later times the formation of *F* at 571 nm. The decay of *F* was relatively slow (1–1.5 ms, Fig. 1*B*) and was analyzed from the absorbance change at 571–580 nm (Fig. 8). Except for the first 100–200 μs, in which these wavelength pairs might contain significant contributions from *A* and P_R, the time course of *F* was satisfactorily reproduced. The half-life for the $P_R \rightarrow F$ protonation was simulated as 27 μs, identical to the value in a previous study (38). The value of 27 μs was, however, not determined directly from the time course of F, but was constrained to adequately fit the Cu_A/heme *a* and Trp* kinetics (Figs. 5, 6, and 8). The decay rate of *F*, the $F \rightarrow O_H$ transition, can also be estimated from the oxidation of heme *a* in the α-band at 603 nm and in the Soret region at 444 nm (Fig. 1, *A* and *B*). Furthermore, the 430 nm maximum shifted with a similar rate ($t_{1/2}$ = 1.2 ms) yielding O_H, characterized by the maximum at 427 nm after 3–6 ms (Fig. 1, *A* and *B*). Resonance Raman spectroscopy showed that in the $F \rightarrow O_H$ transition heme a_3 $Fe^{4+}=O$ was reduced by heme a/Cu_A to Fe^{3+}–OH^- (36, 38). The simultaneous oxidation of heme *a* and reduction of heme a_3 is very difficult to analyze by UV-visible spectroscopy. The rate of the $F \rightarrow O_H$ transition was calculated from the second oxidation phase ($t_{1/2}$ = 1.2 ms) of heme *a* and Cu_A and from the formation rate of the Trp-272* all three monitored by EPR spectroscopy (Figs. 5, 6, and 8).

The majority of the high spin heme a_3 Fe^{3+}(–OH^-) was EPR-silent under all conditions examined. Likewise the characteristic four-line EPR signal of Cu_B^{2+}–OH^- was not observed in any of the MHQ samples even though the experimental conditions were optimized for its detection. This specific Cu_B^{2+}–OH^- state has been observed in low temperature kinetics ("triple trapping experiments") of the bovine heart CcO and has been assigned to the P_R intermediate (42). The Cu_B EPR signal is absent in *F* (67). The four-line EPR spectrum was suggested to disappear due to *e.g.* protonation of Cu_B^{2+}–OH^- or of another base close to the binuclear center, which would slightly change the magnetic interaction with $Fe^{4+}=O$ to a value rendering Cu_B^{2+} EPR invisible (42). Thus, although our UV-visible spectra indicate formation of P_R, our EPR data did not seem to support this. A possible explanation might be that the magnetic interaction in the *P. denitrificans* CcO differs from the bovine heart enzyme yielding an EPR-silent Cu_B^{2+} in P_R. We consider it, however, more likely that the protonation of Cu_B (and other) equilibria are somewhat different at the low temperatures employed in the triple-trapping method (40, 42, 67) compared with 10 °C in our experiments. This could lead to accumulation of different intermediates and rendering Cu_B^{2+} EPR-silent. Such a shift in equilibria might also explain why the Trp-272* has not been observed in the triple trapping experiments (40, 42, 67).

Heme a and Cu_A Kinetics and Equilibrium—The biphasic oxidation kinetics of heme *a* and Cu_A determined by EPR (Fig. 6) displayed an initial phase completed within ~130/200 μs (*apparent* $t_{1/2}$ = 55 μs), whereas the decay half-life of the second phase equaled 1.2 ms. This biphasic time course and the half-lives were in perfect agreement with the kinetics of the two electrogenic events of the *P. denitrificans* CcO (68, 69). In each oxidation phase a *single* electron from the heme *a*/Cu_A redox pair was donated to the binuclear center (Figs. 6 and 8).

Heme *a* oxidation proceeded on the nanosecond time scale (43) in the $P_M \rightarrow P_R$ transition (Fig. 7), but the apparent $t_{1/2}$ values for Cu_A and heme *a* were 50 μs and 65 μs, respectively (Fig. 6, *inset*). These latter *apparent* half-lives are upper limits with respect to the true $Cu_A \Leftrightarrow$ heme *a* electron transfer rates, because the preceding formation of $R \rightarrow P_M$ takes ~30–50 μs both for the bovine heart CcO (28, 35, 36, 38) and the *P. denitrificans* enzyme (68, 69). The half-life for $Cu_A \rightarrow$ heme *a* electron transfer has been determined at $t_{1/2}$ = 24 and 35 μs for the *R. sphaeroides* and *P. denitrificans* CcOs, respectively (66, 70). The actual freezing time of the MHQ is 30–40 μs and because the heme *a* → heme a_3 electron transfer rate is in nanoseconds, the finding of similar degrees of reduction for Cu_A and heme *a* strongly suggested that they are in electronic equilibrium at all measured reaction times (Fig. 3). The calculated equilibrium constant indicated a 4.5-mV lower midpoint potential for Cu_A relative to heme *a* in good agreement with a previous study (66). The lower reduction potential of Cu_A led to a slightly faster apparent oxidation of Cu_A relative to heme *a*. In contrast, in the bovine heart CcO the oxidation of heme *a* is apparently faster than of Cu_A (38).

The second oxidation phase of Cu_A/heme *a* was slow ($t_{½}$ = 1.2 ms) and gated by the slow $F \rightarrow F_W$* reaction (Fig. 7). The reduction of Trp-272* occurred with $t_{½}$ = 60 μs (Figs. 5 and 7) by electron transfer from Cu_A/heme *a*. The value of 60 μs represents most likely electron transfer from Cu_A to heme *a*. So the rates of $Cu_A \Leftrightarrow$ heme *a* electron transfer are actually very similar in the two oxidation phases, $t_{½}$ = ~30 μs in the first phase and 60 μs in the second. Both rates are similar to measured (70) and calculated (71) electron transfer rates for Cu_A to heme *a*. The approximate 2-fold difference of $t_{½}$ in the two phases might reflect small differences in the effective reduction potentials and reorganization energies (totaling ~20 mV) for each oxidation phase.

Identification of Trp as Trp-272**—EPR spectroscopy revealed two different radicals (Figs. 2–5). The origin of the 6-ms radical could not be established. Likewise, its functional assignment was difficult even though it was being formed on the time scale of turnover. The kinetics of the 6-ms radical, which accumulated to 0.5% of the CcO, could not be accurately established due to spectral overlap with the Trp-272*. However, the observation that two radicals are formed on the time scale of turnover indicates rapid radical migration within CcO (46).

The Q-band spectrum of the radical formed maximally after 300–500 μs can be firmly assigned as a Trp*. The EPR and electron nuclear double resonance properties of Trp radicals are well understood. All Trp radicals have similar hyperfine constants for the indole ring protons (H5 and H7) and the indole nitrogen and show similar small *g*-anisotropies (60, 62). The major differences in Trp* EPR spectra are caused by variations in the angles of the two β-methylene protons ($H\beta_1$ and $H\beta_2$) with respect to the indole ring, which strongly affects their hyperfine values (62). The relation between the ratio of the hyperfine values of the two β-methylene protons and the angles can be calculated with the McConnnel relation and thus permits assignment of the Trp* residue in case the crystal structure is known (62). Furthermore, EPR can distinguish between a neutral Trp* and a protonated Trp*.

The hyperfine constants for the indole ring protons and nitrogen used for the Trp* simulation (Fig. 4 and Table 1) are very similar to those of other Trp* (62). The best fitting values for the two β-methylene protons (25 and 7.5 Gauss) correspond to angles of 3.1° and 123.1° (calculated from the ratio $H\beta_1/H\beta_2$) characterizing the radical as that from Trp-272 (Table 1). However, given the signal-to-noise level in the Q-band spectrum (Fig. 4), which required averaging of 85 spectra, because the absolute Trp* concentration was only 1.4 μM, we need to discuss possible other Trp residues as the origin of the Trp*. In particular, simulated EPR spectra in which the ratio $H\beta_2/H\beta_1$ would be close to zero (Trp-358 and Trp-431, Table 1) are not entirely inconsistent with the experimental spectrum (see supplemental Fig. S3). Our observation that the Trp* is also formed in the *E. coli* cytochrome bo_3 (5, 46), implies that it concerns a Trp residue conserved in the *P. denitrificans* and *E. coli* oxidases. There are 12 Trp residues in subunit I conserved between these two enzymes. Table 1 lists nine Trp residues conserved in the Type A1 oxidases, their distances to the metal sites, and their predicted ratios of the β-methylene proton hyperfine constants. The highly conserved Trp-164 was ruled out because the radical was found to be present in W164F and W164T mutants (data not shown). Trp-323, although close enough to heme a_3 (and Cu_B) was ruled out on the basis of its predicted EPR spectrum, which would show a strong central line (*cf.* supplemental Fig. S3), in contrast to experimental observations. Residues Trp-22, Trp-136, Trp-431, and Trp-532 are judged too far from any of the metal centers to produce the magnetic coupling dominating the X-band EPR spectral features. In terms of its predicted EPR spectrum (supplemental Fig. S3) and the 15- to 16-Å distance to heme a_3, which might lead to a weak magnetic coupling, Trp-358 is the only other serious candidate apart from Trp-272. However, Trp-358 is a phenylalanine residue in the *Aeropyrum pernix* oxidase and is not conserved in Type A2, Type B, and Type C oxidases (7). We ascribe the observed radical to the Trp-272*, because 1) the Q-band EPR spectrum is optimally simulated as a Trp-272*, 2) Trp-272 is close to all three metal centers in subunit I, and 3) Trp-272 is strictly conserved in all cytochrome oxidases. The Q-band EPR spectrum could not be simulated as a protonated Trp-272* (72), and we therefore conclude that the species represents the neutral Trp-272*. A weak H-bond interaction of the indole-N with another residue, however, can not be ruled out. In fact the phenol–OH of Tyr-167 and the indole-N of Trp-272 are within H-bonding distance (3, 8).

In contrast to the Q-band spectrum, the four-line X-band EPR spectrum of Trp-272* (Fig. 4) could not be simulated. With respect to our previous analysis (46) we know now, on the basis of the Q-band spectrum, that this spectrum does not contain contributions from a Tyr* as suggested at the time, although it does contain a small contribution from the 6-ms radical (Figs. 3 and 4). The rapid relaxation of the Trp* (46) and the increased resolution at Q-band indicate that the Trp-272* is weakly magnetically coupled as proposed earlier. Simulation of the X-band EPR spectrum would require a full diagonalization of the spin Hamiltonian matrix, because the various magnetic interactions, including the Zeeman interaction, are in the same order of magnitude. This most complicated EPR-simulation scenario is outside the scope of this report.

The Function of the Trp-272 in the Catalytic Cycle*—Our current view on the catalytic cycle of cytochrome oxidases is depicted in Fig. 7. The half-lives of the various intermediates indicated were used for simulation of Cu_A/heme *a* and Trp-272* kinetics (Figs. 5, 6, and 8) with values for $R \rightarrow P_M/P_R$ taken from the literature. Maximal Trp-272* formation occurs after 300–500 μs, to an extent of 4–5% of the oxidase. This low extent is due to an ~20-fold lower rate of formation ($t_{½}$ = 1.2 ms) than rate of breakdown (60 μs). The low formation rate may seems to preclude a direct role of Trp-272 as electron donor in the O=O bond splitting reaction ($A \rightarrow P_M$) as suggested recently (44). However, any radical formed in this reaction (Tyr-280* or Trp-272*) would most likely accumulate to undetectable levels (like P_M, Fig. 8) given the ~1-ns rate of electron transfer from heme *a* to heme a_3. Thus while Trp-272 might nevertheless play a role in the O=O bond breaking (*cf.* Ref. 44), our data suggest another role in the catalytic cycle.

The intermediate *F* accumulates to ~88% of the CcO concentration (Fig. 8 and Ref. 38), because it was formed with an

apparent $t_{1/2} \sim 100\ \mu s$ and decays in 1.2 ms, approximately the opposite of the kinetic parameters calculated for Trp-272*. Unless the quantitation of the X-band EPR spectrum of Trp-272* is off by a factor of 20, the accumulation of Trp-272* to 4–5% implies that Trp-272* is not present in *F* (Fig. 8) and, in addition, that it is formed later than *F*. We therefore propose the new sequence $F \rightarrow F_W^* \rightarrow O_H$ (Fig. 7). The simulation of the kinetics allows for ~88% accumulation of *F* and ~4% of F_W^* (Fig. 8). The low accumulation of F_W^* might explain why it has not been detected hitherto by UV-visible or resonance Raman spectroscopy, even though several authors have proposed additional intermediates in the $F \rightarrow O_H$ reaction sequence (28, 51, 73, 74).

Formation of the neutral Trp-272* with $t_{1/2} = 1.2$ ms represents the major rate determining step in the CcO catalytic cycle. The Trp-272* is obtained according to Reaction 2.

$$\text{Trp-272} \rightarrow \text{Trp-272*} + e + H^+$$

REACTION 2

Which are the electron and proton acceptors for Trp-272? Potential electron acceptors are heme a_3 $Fe^{4+}=O$ and Cu_B^{2+}–OH^-. Regarding Cu_B, its reduction to Cu_B^{1+}–OH_2 would explain its EPR silence. In the next step, Cu_B^{1+} would reduce $Fe^{4+}=O$ while Trp-272* is re-reduced to Trp-272 by the electron residing in the Cu_A/heme *a* redox pair. This sequence of events would explain why heme a_3 and Cu_B are EPR-silent in F_W^* and O_H. In the alternative route (shown in Fig. 7) Trp-272 is suggested as the direct reductant to heme a_3 $Fe^{4+}=O$ yielding Fe^{3+}–OH^-. The Trp-272* is subsequently re-reduced to Trp-272 by electron transfer from Cu_A/heme *a*. In both scenarios, the metal ions can accept the proton (Reaction 2) upon their reduction. Our data and those availing in the literature do not appear to distinguish between these two alternatives in part due to the spectroscopic silence of Cu_B. However, resonance Raman spectroscopy indicates the formation of Fe^{3+}–OH^- prior to Fe^{3+} (38). According to the literature, the electron donors Cu_A/heme *a* reduce heme a_3 $Fe^{4+}=O$ to Fe^{3+}–OH^-. The source of the proton in this reaction remains unknown. In Fig. 7, Trp-272 is indicated to act as the electroneutral reductant to $Fe^{4+}=O$. *However*, instead of Trp-272 the conserved Glu-278 might be the direct proton donor in the reduction (by Trp-272) of $Fe^{4+}=O$ to Fe^{3+}–OH^- (in $F \rightarrow F_W^*$), whereas the proton from Trp-272 (Reaction 2) is expelled to the periplasm, according to Reaction 3.

$$\text{Trp-272} + \text{Glu-278-COOH} + Fe^{4+}=O \rightarrow \text{Trp-272*} + H^+_{peri} + \text{Glu-278-COO}^- + Fe^{3+}\text{-}OH^-$$

REACTION 3

Reprotonation of Glu-278$^-$ occurs via the D-pathway by proton uptake form the cytoplasm.

The short distance of Trp-272 to Cu_B or heme a_3 (Table 1) would in any case ensure submillisecond to millisecond electron transfer rates even when the reduction potentials of the redox partners differ by 0.4 V (71). The 1.2-ms rate of Reaction 2 thus suggests a reduction potential of 0.7–0.8 V for Trp-272, a value lower than the ~0.9 V and ~1.1 V for free Trp in solution (pH 7) or buried, respectively (75), but adequate to play a role in O=O bond breaking and as reductant to heme a_3 or Cu_B.

In the reverse of Reaction 2 the strong base Trp-272$^-$ ($pK_a >$ 15, *cf.* Ref. 75) is formed initially by electron transfer from Cu_A/heme *a*. The Trp-272$^-$ anion might subsequently be rapidly protonated to Trp-272 by a proton *en route* from the cytoplasm to the periplasm, thus providing directionality to proton translocation (in $F \rightarrow O_H$). The conserved Glu-278 might serve as the direct proton donor to the Trp-272$^-$ anion according to Reaction 4.

$$\text{Trp-272}^- + \text{Glu-278-COOH} \rightarrow \text{Trp-272} + \text{Glu-278-COO}^-$$

REACTION 4

Reactions 3 and 4, combined, describe (part of) a proton-relay network in which protons are translocated from the cytoplasm to the periplasm thermodynamically driven by the oxidoreduction of Trp-272 and the strong basicity of the Trp-272$^-$ anion.

Electrometric and proton translocation measurements have provided ample evidence for proton pumping in the $F \rightarrow O_H$ transition (9, 12, 39, 58, 68), which we here propose to occur actually in the $F_W^* \rightarrow O_H$ transition involving Trp-272. For the $P_R \rightarrow F$ transition, a proton acceptor was suggested to be located close to or at the heme a_3 propionates, but not at the heme a_3-Cu_B binuclear center (9, 12, 39, 58, 68). The Trp-272$^-$ anion fits both the proton acceptor properties and the proposed location.

In view of our findings, the concept of cytochrome oxidase as a redox-linked proton pump (9, 68) might thus be extended. Although the various metal centers are engaged in oxidation-reduction-linked deprotonation-protonation reactions, specific aromatic residues like the strictly conserved Trp-272 (and possibly Tyr-280) also change their redox- and protonation states during the catalytic cycle and are likewise involved in proton binding, proton release, and proton translocation. In contrast to the metal ions of the binuclear center, the aromatic residues are not directly involved in the binding (and activation) of O_2. According to the model presented here, formation of the Trp-272$^-$ anion provides the driving force for proton binding and even translocation in the $F_W^* \rightarrow O_H$ transition and, thus, constitutes an integral part of a proton-relay network in the cytochrome oxidases. Whether a similar mechanism applies to the $P_R \rightarrow F$ transition and to the two proton-pumping events in the reductive part of the catalytic cycle, and whether it would involve Trp-272 as well, are subject to future experimentation.

Acknowledgments—We thank Werner Müller (Frankfurt) for enzyme preparation, and Marc J. F. Strampraad (Delft) and A. Paulus (Delft) for help with the kinetic experiments. We further acknowledge the constructive comments of one of the reviewers.

REFERENCES

1. Wasser, I. M., de Vries, S., Moënne-Loccoz, P., Schröder, I., and Karlin, K. D. (2002) *Chem. Rev.* **102,** 1201–1234
2. Richter, O. M. H., and Ludwig, B. (2003) *Rev. Physiol. Biochem. Pharmacol.*

147, 47–74
3. Michel, H., Behr, J., Harrenga, A., and Kannt, A. (1998) *Annu. Rev. Biophys. Biomol. Struct.* **27,** 329–356
4. Hendriks, J., Oubrie, A., Castresana, J., Urbani, A., Gemeinhardt, S., and Saraste, M. (2000) *Biochim. Biophys. Acta* **1459,** 266–273
5. Cherepanov, A. V., and De Vries, S. (2004) *Biochim. Biophys. Acta* **1656,** 1–31
6. Babcock, G. T., and Wikstrom, M. (1992) *Nature* **356,** 301–309
7. Pereira, M. M., Santana, M., and Teixeira, M. (2001) *Biochim. Biophys. Acta* **1505,** 185–208
8. Ostermeier, C., Harrenga, A., Ermler, U., and Michel, H. (1997) *Proc. Natl. Acad. Sci. U. S. A.* **94,** 10547–10553
9. Wikstrom, M. (2004) *Biochim. Biophys. Acta* **1655,** 241–247
10. Verkhovsky, M. I., Belevich, I., Bloch, D. A., and Wikstrom, M. (2006) *Biochim. Biophys. Acta* **1757,** 401–407
11. Ruitenberg, M., Kannt, A., Bamberg, E., Fendler, K., and Michel, H. (2002) *Nature* **417,** 99–102
12. Faxen, K., Gilderson, G., Adelroth, P., and Brzezinski, P. (2005) *Nature* **437,** 286–289
13. Belevich, I., Verkhovsky, M. I., and Wikstrom, M. (2006) *Nature* **440,** 829–832
14. Iwata, S., Ostermeier, C., Ludwig, B., and Michel, H. (1995) *Nature* **376,** 660–669
15. Tsukihara, T., Aoyama, H., Yamashita, E., Tomizaki, T., Yamaguchi, H., Shinzawa-Itoh, K., Nakashima, R., Yaono, R., and Yoshikawa, S. (1995) *Science* **269,** 1069–1074
16. Svensson-Ek, M., Abramson, J., Larsson, G., Tornroth, S., Brzezinski, P., and Iwata, S. (2002) *J. Mol. Biol.* **321,** 329–339
17. Yoshikawa, S., Muramoto, K., Shinzawa-Itoh, K., Aoyama, H., Tsukihara, T., Ogura, T., Shimokata, K., Katayama, Y., and Shimada, H. (2006) *Biochim. Biophys. Acta* **1757,** 395–400
18. Yoshikawa, S., Muramoto, K., Shinzawa-Itoh, K., Aoyama, H., Tsukihara, T., Shimokata, K., Katayama, Y., and Shimada, H. (2006) *Biochim. Biophys. Acta* **1757,** 1110–1116
19. Witt, H., Malatesta, F., Nicoletti, F., Brunori, M., and Ludwig, B. (1998) *J. Biol. Chem.* **273,** 5132–5136
20. Drosou, V., Malatesta, F., and Ludwig, B. (2002) *Eur. J. Biochem.* **269,** 2980–2988
21. Blackburn, N. J., Barr, M. E., Woodruff, W. H., van der Oost, J., and de Vries, S. (1994) *Biochemistry* **33,** 10401–10407
22. Brzezinski, P. (2004) *Trends Biochem. Sci.* **29,** 380–387
23. Adelroth, P., Ek, M. S., Mitchell, D. M., Gennis, R. B., and Brzezinski, P. (1997) *Biochemistry* **36,** 13824–13829
24. Schmidt, B., McCracken, J., and Ferguson-Miller, S. (2003) *Proc. Natl. Acad. Sci. U. S. A.* **100,** 15539–15542
25. Schmidt, B., Hillier, W., McCracken, J., and Ferguson-Miller, S. (2004) *Biochim. Biophys. Acta* **1655,** 248–255
26. Florens, L., Schmidt, B., McCracken, J., and Ferguson-Miller, S. (2001) *Biochemistry* **40,** 7491–7497
27. Espe, M. P., Hosler, J. P., Ferguson-Miller, S., Babcock, G. T., and McCracken, J. (1995) *Biochemistry* **34,** 7593–7602
28. Szundi, I., Cappuccio, J., and Einarsdottir, O. (2004) *Biochemistry* **43,** 15746–15758
29. Sucheta, A., Szundi, I., and Einarsdottir, O. (1998) *Biochemistry* **37,** 17905–17914
30. Sucheta, A., Georgiadis, K. E., and Einarsdottir, O. (1997) *Biochemistry* **36,** 554–565
31. Einarsdottir, O., and Szundi, I. (2004) *Biochim. Biophys. Acta* **1655,** 263–273
32. Varotsis, C., Zhang, Y., Appelman, E. H., and Babcock, G. T. (1993) *Proc. Natl. Acad. Sci. U. S. A.* **90,** 237–241
33. Proshlyakov, D. A., Pressler, M. A., and Babcock, G. T. (1998) *Proc. Natl. Acad. Sci. U. S. A.* **95,** 8020–8025
34. Proshlyakov, D. A., Ogura, T., Shinzawa-Itoh, K., Yoshikawa, S., Appelman, E. H., and Kitagawa, T. (1994) *J. Biol. Chem.* **269,** 29385–29388
35. Ogura, T., and Kitagawa, T. (2004) *Biochim. Biophys. Acta* **1655,** 290–297
36. Kitagawa, T. (2000) *J. Inorg. Biochem.* **82,** 9–18
37. Han, S. W., Ching, Y. C., and Rousseau, D. L. (1990) *Proc. Natl. Acad. Sci. U. S. A.* **87,** 2491–2495
38. Han, S., Takahashi, S., and Rousseau, D. L. (2000) *J. Biol. Chem.* **275,** 1910–1919
39. Siletsky, S. A., Han, D., Brand, S., Morgan, J. E., Fabian, M., Geren, L., Millett, F., Durham, B., Konstantinov, A. A., and Gennis, R. B. (2006) *Biochim. Biophys. Acta* **1757,** 1122–1132
40. Hansson, O., Karlsson, B., Aasa, R., Vanngard, T., and Malmstrom, B. G. (1982) *EMBO J.* **1,** 1295–1297
41. Proshlyakov, D. A., Pressler, M. A., DeMaso, C., Leykam, J. F., DeWitt, D. L., and Babcock, G. T. (2000) *Science* **290,** 1588–1591
42. Morgan, J. E., Verkhovsky, M. I., Palmer, G., and Wikstrom, M. (2001) *Biochemistry* **40,** 6882–6892
43. Pilet, E., Jasaitis, A., Liebl, U., and Vos, M. H. (2004) *Proc. Natl. Acad. Sci. U. S. A.* **101,** 16198–16203
44. MacMillan, F., Budiman, K., Angerer, H., and Michel, H. (2006) *FEBS Lett.* **580,** 1345–1349
45. Bloch, D., Belevich, I., Jasaitis, A., Ribacka, C., Puustinen, A., Verkhovsky, M. I., and Wikstrom, M. (2004) *Proc. Natl. Acad. Sci. U. S. A.* **101,** 529–533
46. Wiertz, F. G. M., Richter, O. M. H., Cherepanov, A. V., MacMillan, F., Ludwig, B., and de Vries, S. (2004) *FEBS Lett.* **575,** 127–130
47. Lu, S., Wiertz, F. G. M., de Vries, S., and Moenne-Loccoz, P. (2005) *J. Raman Spectrosc.* **36,** 359–362
48. Wiertz, F. G. M., and de Vries, S. (2006) *Biochem. Soc. Transact.* **34,** 136–138
49. Ballou, D. P. (1978) *Methods Enzymol.* **54,** 85–93
50. Rigby, S. E., Junemann, S., Rich, P. R., and Heathcote, P. (2000) *Biochemistry* **39,** 5921–5928
51. Rich, P. R., Rigby, S. E., and Heathcote, P. (2002) *Biochim. Biophys. Acta* **1554,** 137–146
52. Fabian, M., and Palmer, G. (1995) *Biochemistry* **34,** 13802–13810
53. Ludwig, B. (1986) *Methods Enzymol.* **126,** 153–159
54. Hendler, R. W., Pardhasaradhi, K., Reynafarje, B., and Ludwig, B. (1991) *Biophys. J.* **60,** 415–423
55. Käss, H., MacMillan, F., Ludwig, B., and Prisner, T. F. (2000) *J. Phys. Chem. B* **104,** 5362–5371
56. Budiman, K., Kannt, A., Lyubenova, S., Richter, O. M. H., Ludwig, B., Michel, H., and MacMillan, F. (2004) *Biochemistry* **43,** 11709–11716
57. von Wachenfeldt, C., de Vries, S., and van der Oost, J. (1994) *FEBS Lett.* **340,** 109–113
58. Salomonsson, L., Faxen, K., Adelroth, P., and Brzezinski, P. (2005) *Proc. Natl. Acad. Sci. U. S. A.* **102,** 17624–17629
59. Nyquist, R. M., Heitbrink, D., Bolwien, C., Gennis, R. B., and Heberle, J. (2003) *Proc. Natl. Acad. Sci. U. S. A.* **100,** 8715–8720
60. Pogni, R., Baratto, M. C., Teutloff, C., Giansanti, S., Ruiz-Duenas, F. J., Choinowski, T., Piontek, K., Martinez, A. T., Lendzian, F., and Basosi, R. (2006) *J. Biol. Chem.* **281,** 9517–9526
61. Lendzian, F., Sahlin, M., MacMillan, F., Bittl, R., Fiege, R., Potsch, S., Sjoberg, B.-M., Graslund, A., Lubitz, W., and Lassmann, G. (1996) *J. Am. Chem. Soc.* **118,** 8111–8120
62. Bleifuss, G., Kolberg, M., Potsch, S., Hofbauer, W., Bittl, R., Lubitz, W., Graslund, A., Lassmann, G., and Lendzian, F. (2001) *Biochemistry* **40,** 15362–15368
63. Svistunenko, D. A., Wilson, M. T., and Cooper, C. E. (2004) *Biochim. Biophys. Acta* **1655,** 372–380
64. Ivancich, A., Jakopitsch, C., Auer, M., Un, S., and Obinger, C. (2003) *J. Am. Chem. Soc.* **125,** 14093–14102
65. Ivancich, A., Dorlet, P., Goodin, D. B., and Un, S. (2001) *J. Am. Chem. Soc.* **123,** 5050–5058
66. Farver, O., Grell, E., Ludwig, B., Michel, H., and Pecht, I. (2006) *Biophys. J.* **90,** 2131–2137
67. Blair, D. F., Witt, S. N., and Chan, S. I. (1985) *J. Am. Chem. Soc.* **107,** 7389–7399
68. Wikstrom, M., and Verkhovsky, M. I. (2006) *Biochim. Biophys. Acta* **1757,** 1047–1051
69. Ribacka, C., Verkhovsky, M. I., Belevich, I., Bloch, D. A., Puustinen, A., and Wikstrom, M. (2005) *Biochemistry* **44,** 16502–16512

70. Adelroth, P., Brzezinski, P., and Malmstrom, B. G. (1995) *Biochemistry* **34,** 2844–2849
71. Moser, C. C., Page, C. C., and Dutton, P. L. (2006) *Philos. Trans. R. Soc. Lond B Biol. Sci.* **361,** 1295–1305
72. Baldwin, J., Krebs, C., Ley, B. A., Edmondson, D. E., Huynh, B. H., and Bollinger, J. M. (2000) *J. Am. Chem. Soc.* **122,** 12195–12206
73. Zaslavsky, D., Smirnova, I. A., Adelroth, P., Brzezinski, P., and Gennis, R. B. (1999) *Biochemistry* **38,** 2307–2311
74. Pecoraro, C., Gennis, R. B., Vygodina, T. V., and Konstantinov, A. A. (2001) *Biochemistry* **40,** 9695–9708
75. Tommos, C., Skalicky, J. J., Pilloud, D. L., Wand, A. J., and Dutton, P. L. (1999) *Biochemistry* **38,** 9495–9507
76. Fersht, A. (1999) *Structure and Mechanism in Protein Science: A Guide to Enzyme Catalysis and Protein Folding*, W.H. Freeman and Company, NY